Reduced noise temperatures of a THz NbN Hot Electron Bolometer Mixer

Mirzaei, B.; Silva, J. R.G.; Vreeling, W. J.; Laauwen, W.; Ren, D.; Gao, J. R.

DOI
10.1109/TTHZ.2024.3475010

Publication date
2025

Document Version
Final published version

Published in
IEEE Transactions on Terahertz Science and Technology

Reduced Noise Temperatures of a THz NbN Hot Electron Bolometer Mixer

Behnam Mirzaei, Jose R. G. Silva, Willem-Jan Vreeling, Wouter M. Laauwen, Dingding Ren, and Jian-Rong Gao

***Abstract*—In this article, we measure the double sideband (DSB) receiver noise temperature ($T_{\text{rec}}^{\text{DSB}}$) of an NbN hot electron bolometer (HEB) mixer at three local oscillator frequencies of 1.6, 2.5, and 5.3 THz. The HEB has cleaned contact interfaces with a 200-nm-thick Au layer. The measured $T_{\text{rec}}^{\text{DSB}}$ values are 530 ± 11 K, 640 ± 18 K, and 2190 ±150 K at 1.6, 2.5, and 5.3 THz, respectively, using an air setup with total optical losses of 2.60 ± 0.04, 2.63 ± 0.16, and 4.70 ± 0.24 dB, respectively. We derived low mixer noise temperatures ($T_{\text{mixer}}^{\text{DSB}}$) of 240 ± 6 K at 1.6 THz and 290 ± 13 K at 2.5 THz, achieving over 30% improvement compared to published NbN HEB mixers. This enhancement can reduce the integration time of a heterodyne instrument by roughly a factor of 2. At 5.3 THz, $T_{\text{mixer}}^{\text{DSB}}$ is 620 ± 55 K, showing limited improvement due to nonoptimized antenna geometry. These results also contribute to understanding the device physics of a wide HEB (4 μm) at high frequencies. The mixer was developed for the proposed Orbiting Astronomical Satellite for Investigating Stellar Systems and Single Aperture Large Telescope for Universe Studies (concept) missions.**

***Index Terms*—Hot electron bolometer (HEB) mixer, low noise, NbN, spiral antenna, terahertz.**

I. Introduction

HOT electron bolometer (HEB) mixers based on a thin NbN superconducting bridge are, so far, the most sensitive heterodyne detectors for high-spectral-resolution ($\geq 10^6$) spectroscopy in astronomical observations within the frequency range of 1–6 THz. Due to water vapor absorption in the atmosphere, such observations can only be realized through air-, balloon-, and space-borne observatories. NbN HEBs have been flown, for example, on HIFI-Herschel [1], SOFIA [2], STO2 [3], GUSTO [4], and ASTHROS (to be flown) [5]. They are also the choice for far-infrared spectroscopic surveyor (or line emission terahertz observatory (LETO)) [6], Orbiting Astronomical Satellite for Investigating Stellar System (OASIS) [7], and Single Aperture Large Telescope for Universe Studies (SALTUS) [8] space missions, proposed to the European Space Agency or National Aeronautics and Space Administration (NASA). Notably, due to the limited lifetime of a space mission, a low mixer noise temperature ($T_{\text{mixer}}^{\text{DSB}}$) is highly desirable to optimize observation time as the integration time of the heterodyne instruments is proportional to the square of the receiver noise temperature [($T_{\text{rec}}^{\text{DSB}}$), which is the sensitivity of a mixer including the contribution from all the optical components] [9].

Many years of research and development at various research groups in the world have been devoted to realizing, understanding, and improving low-noise NbN HEBs [10], [11], [12]. Here, we only quote the sensitivities for one frequency, namely, $T_{\text{rec}}^{\text{DSB}}$, measured at 1.6 THz or extrapolated to this frequency, which is, for example, 750 K from HIFI [1], 690 K from STO2 [13], and 760 K from GUSTO [14]. $T_{\text{rec}}^{\text{DSB}}$ has not been reduced in the past decade. The HEBs for STO2 [13] and GUSTO [14] were fabricated at TU Delft/SRON, using contacts with a superconducting interlayer of either NbTiN [15] or Nb [16] between thin Au and ultrathin NbN layers. This interlayer helps mitigate the proximity effect, maintaining the superconductivity of the NbN underneath the Au and preventing the reduction of the critical temperature (T_c) of the NbN bridge. However, the interlayer may introduce side effects, such as RF loss, which can impact $T_{\text{mixer}}^{\text{DSB}}$.

The development of Au contacts for NbN HEBs, with efforts to improve interface quality, has been reported in [17] and [18]. In [17], thin Au contacts (15 nm) were created using an in situ process, where the Au layer was sputter deposited immediately after the growth of the NbN film, without breaking the vacuum. This work reported a minimal $T_{\text{rec}}^{\text{DSB}}$ of 600 K at 2.5 THz; however, a detailed breakdown of the different noise contributions was not provided. Furthermore, it remains unclear if the in situ process results in a highly transparent interface between Au and NbN, as the interface quality depends on factors such as the vacuum conditions, the waiting time before Au deposition, and the presence or absence of an adhesion layer.

The approach in [18] differs by using Ar^+ plasma to clean the surface of the NbN film in the contact areas, followed by the in situ evaporation of a thick Au layer (200 nm) with a thin Ti

Received 26 November 2023; revised 22 February 2024, 19 April 2024, 29 June 2024, and 14 August 2024; accepted 24 September 2024. Date of publication 7 October 2024; date of current version 8 January 2025. This work was supported in part by The Netherlands Organization for Scientific Research under Grant 614.061.609, in part by EU RADIOBLOCKS project under Grant 101093934, and in part by TU Delft Space Institute. *(Corresponding authors: Jian-Rong Gao; Behnam Mirzaei.)*

Behnam Mirzaei and Dingding Ren are with the Department of Imaging Physics, Delft University of Technology, 2628 CJ Delft, The Netherlands (e-mail: bmmi.644@gmail.com; d.ren-1@tudelft.nl).

Jose R. G. Silva, Willem-Jan Vreeling, and Wouter M. Laauwen are with SRON Netherlands Institute for Space Research, 9747 AD Groningen, The Netherlands (e-mail: j.r.g.d.silva@sron.nl; w.j.vreeling@sron.nl; w.m.laauwen@sron.nl).

Jian-Rong Gao is with the Department of Imaging Physics, Delft University of Technology, 2333 CA Leiden, The Netherlands, and also with SRON Netherlands Institute for Space Research,, 2628 CJ Delft, The Netherlands (e-mail: j.r.gao@sron.nl).

Color versions of one or more figures in this article are available at https://doi.org/10.1109/TTHZ.2024.3475010.

Digital Object Identifier 10.1109/TTHZ.2024.3475010

adhesion layer. These HEBs demonstrated a minimal $T_{\text{rec}}^{\text{DSB}}$ of 780 K at 2.5 THz. The critical step in this process is determining the amount of surface material of the NbN that should be etched away.

Here, we present the results of a new NbN HEB mixer with contacts that were Ar^+ cleaned and in situ evaporated with a thick Au layer, following a method like in [18]. We demonstrate that $T_{\text{mixer}}^{\text{DSB}}$ improves by roughly 30% at 1.6 and 2.5 THz compared to our previously reported results for HEBs using Au/Nb (or NbTiN) superconducting contacts. We measured $T_{\text{rec}}^{\text{DSB}}$ and receiver conversion loss ($L_{\text{rec}}^{\text{DSB}}$) at three frequencies: 1.6, 2.5, and 5.3 THz, and determined $T_{\text{mixer}}^{\text{DSB}}$ and the mixer conversion loss ($L_{\text{mixer}}^{\text{DSB}}$). The last two provide valuable and crucial data for the practical application of HEBs in observatories and for understanding their ultimate heterodyne performance.

The aim of this study is also to demonstrate sensitive HEB mixers for the SALTUS mission [8], which requires three arrays of HEBs operating in distinct frequency ranges: the 1–2 THz band for various molecules, such as H_2O lines; a single frequency of 2.67 THz for the HD (1–0) line; and a single frequency of 5.33 THz for the HD (2–1) line.

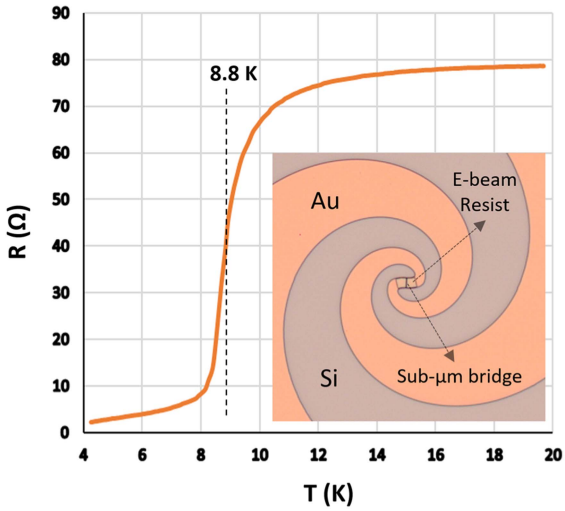

Fig. 1. Resistance versus temperature around the superconducting transition of a 400 nm (length) × 4 μm (width) NbN HEB with cleaned Au/NbN contacts, where the Au is 200 nm thick and forms the spiral antenna. The measurement was conducted using a 1-μA current. Inset: optical micrograph of the device, showing the spiral arms around the NbN bridge.

II. HEB Geometry and Fabrication

The antenna used in [19] and in GUSTO [20] was modified to accommodate the bridge, which is twice as wide at its center. The log spiral (defined by $R = R_0 \exp(\alpha.\ \phi)$, where R is the distance from the center, R_0 is the inner radius, and ϕ is the azimuthal angle) was adapted and optimized in COMSOL with the following parameters for optimal coupling to the lower frequencies: $R_0 = 4$ μm and $\alpha = 0.39$. The device was fabricated on a 380-μm-thick highly resistive silicon wafer covered with an approximately 5-nm sputtered NbN film[1] with a T_c of 9.9 ± 0.1 K.

The HEB under study, labeled as "OASIS BM2 7B," has a 0.4-μm-long and 4-μm-wide NbN bridge, with a normal state resistance (R_N) of 79 Ω and a T_c of 8.8 ± 0.1 K, embedded in the center of a spiral antenna. We chose the larger size instead of the typical size of a 0.2 μm × 2 μm NbN bridge, as used in [19] and [20], due to the strong lateral proximity effect caused by the contacts, which will be discussed further. Our fabrication method may bring T_c to a lower value, which can affect the local oscillator (LO) power and the operating temperature. We aim for an LO power of around 200 nW, which is desirable for receiver stability and the availability of power from existing LO sources. In addition, we expect wider HEBs to show a lower contact resistance, which could lead to an RF loss.

The spiral antenna, including contact structures, was patterned by the evaporation of a 200-nm-thick Au layer on the NbN film, followed by a liftoff process. The base pressure before the evaporation was 2 × 10^{-6} mbar. A crucial step involved properly performing in situ Ar^+ milling (cleaning) of the film prior to Au evaporation to ensure that the Au/NbN interface was as transparent as possible. The optimal milling parameters were determined by extensive pretests on a similar NbN film. Specifically, the milling beam voltage was 350 V, the beam current was 38 mA, the acceleration voltage was 600 V, and the discharge voltage was 30 V. The sample rotated at 10 r/min, and the etching duration was 50 s. This process etched the native oxide (assumed) and about 8% of the NbN film, corresponding to approximately 0.4 nm, which was monitored by the change in the sheet resistance of the film.

In contrast to the method of adding a superconducting interlayer (e.g., Nb or NbTiN) between the Au contacts and NbN [15], [16], as used for GUSTO's detectors, we directly deposit a 200-nm-thick Au layer with a 5-nm-thick Ti adhesion layer on the cleaned NbN, which is expected to provide better contacts and thus reduce the loss of the RF current from the antenna to the NbN bridge. Moreover, this approach reduces the number of fabrication steps, making the fabrication more reliable and reproducible.

In the next step, a submicrometer NbN bridge area is masked using a negative E-beam resist, followed by reactive ion etching of the rest of the surface until the remaining bare NbN is fully removed. An optical micrograph of the detector is shown in the inset of Fig. 1.

We measured the resistance versus temperature (R–T) of eight HEBs with lengths varying from 200 to 450 nm. As shown in Fig. 1, a T_c of 8.8 ± 0.1 K for the 400-nm-long HEB was typically found, which is about 1 K lower than the T_c of the original film. Furthermore, from the single transition feature in the R–T curve and the nonzero resistance at 4 K, the contact regions of Au/NbN become fully normal, confirmed through a dedicated test structure (not shown). We also found a T_c as low as 8.2 ± 0.1 K from an HEB with a 200-nm-long bridge. This confirms that a (lateral) proximity effect, together with charge conversion resistance at normal-metal–superconductor interfaces [12], has been induced in the superconducting NbN bridge from the thick Au contacts, weakening its superconductivity. This also suggests a transparent (or clean) interface between Au and NbN in the contacts. In contrast, Tretyakov

[1]The NbN film on Si was provided by Terahertz and Infrared Photonics, Moscow, Russia. We measured the thickness to be 5 nm using high-resolution transmission electron microscopy although the nominal thickness was 3.5 nm.

et al. [17] reported that a 100-nm-long HEB still has a T_c of 9 K. Thus, we observed a stronger suppression of T_c than in [17].

III. Experimental Setup

We applied a heterodyne measurement setup in air to measure receiver noise temperature, which is very similar to the setup reported in [14] and [21]. Specifically, a far-infrared (FIR) gas laser generates the LO signal at three frequencies: 1.63, 2.52, and 5.25 THz, referred to as 1.6, 2.5, and 5.3 THz, respectively, in this article. These frequencies are very close to what are required for SALTUS mixers. A solid-state multiplier source could serve as the LO at 1.6 THz, while THz quantum cascade lasers could be used as the LO for the two higher frequencies. Unfortunately, these sources are not available in our labs.

The FIR gas laser LO power delivered to the HEB is controlled by a swing-arm voice coil actuator positioned in front of the laser. This actuator partially blocks the LO radiation, effectively serving as a variable optical attenuator [22]. The HEB mixer is mounted behind an elliptical silicon lens, which has a semiminor axis (a) of 5 mm, a semimajor axis (b) of 5.235 mm, and an extension (c) from the geometric center of the lens of 1.2 mm. The lens has an antireflection (AR) coating [23], [24] made of 28.6-μm-thick Parylene-C, optimized for 1.6 THz. The lens is like the one used in [14] and [21] and couples the radiation to the antenna. The mixer block is placed in a liquid helium cryostat. The THz signal and the LO pass through an ultra-high-molecular-weight polyethylene (UHMW-PE) window at 300 K and a heat filter (QMC) at 4 K, with a cutoff frequency of 5.8 THz. A 3-μm-thick Mylar beam splitter is used to combine the radiation from a hot or cold (295/77 K) load with that of the LO. The hot and cold loads are needed for the Y-factor measurements to determine $T_{\rm rec}^{\rm DSB}$. The mixer is biased and read out using a bias-T, followed by a cryogenic low-noise SiGe amplifier (LNA) inside the cryostat. Between the bias-T and LNA, there is a circulator to prevent standing waves between the LNA and the HEB. The IF signal is filtered at 1.7 GHz within a band of 80 MHz and further amplified by a room temperature LNA before being measured by a power meter. The noise temperature of the IF chain ($T_{\rm IF}$) is 6.5 K. The mixer block is at a temperature of 4.6 K.

The optical losses (L) of the components in the optical path from the hot/cold load to the HEB antenna are summarized in Table I. The air path is approximately 30 cm long with a relative humidity of $\sim$40%.

The optical loss of the lens ($L_{\rm lens}$) at three different frequencies, as presented in Table I, was simulated using COMSOL by assuming a Gaussian beam as input, which is transmitted and focused on the antenna. We used the actual thickness (28.6 μm) of the AR coating layer, Parylene-C, with the absorption coefficients taken from [23] and [24], and the same elliptical lens shape as in practice but scaled down in size to reduce computation time. The absorption coefficient at room temperature was sourced from [25]. Since the lens operates at 4 K in practice, the absorption in Si is expected to be negligibly low, reducing the loss at 5.3 THz (stated in Table I) to 0.92 dB. Essentially, the optical transmission loss calculated by COMSOL includes all factors, such as the loss due to oblique incidence on the elliptical surface, the effects of the actual AR-coating thickness, nonideal refractive index and absorption of Parylene-C, and the absorption in Si.

It is worth mentioning that the impedance mismatching loss between the antenna and the HEB [19] is neither listed in Table I nor included in the calculation of $T_{\rm mixer}^{\rm DSB}$ and the mixer conversion loss $L_{\rm mixer}^{\rm DSB}$ from the measured $T_{\rm rec}^{\rm DSB}$ and receiver conversion loss $L_{\rm rec}^{\rm DSB}$. The reason for this will be discussed in Section IV.

TABLE I
Optical Losses Are Produced by Air ($L_{\rm AIR}$, Calculated), Where the Error Bars Are Due to Uncertainty in the Optical Path Length From the Hot/Cold Load to the Cryostat's Window, the 3-μm Beam Splitter ($L_{\rm BS}$, Calculated for Circular Polarization), With Error Bars Arising From Uncertainty in Its Thickness, the UHMW-PE Window ($L_{\rm WINDOW}$, Measured Directly By the FIR Laser Lines), QMC Heat Filter ($L_{\rm FILTER}$, Measured), and the Silicon Lens With AR Coating Designed for 1.6 THz ($L_{\rm LENS}$)

LO Frequency	$L_{\rm air}$ (dB)	$L_{\rm BS}$ (dB)	$L_{\rm window}$ (dB)	$L_{\rm filter}$ (dB)	$L_{\rm lens}$ (dB)	Total (dB)
1.63 THz	0.64 ±0.02	0.09 ±0.01	0.38 ±0.02	1.14 ±0.02	0.35 ±0.02	2.60 ±0.04
2.52 THz	0.38 ±0.01	0.19 ±0.02	0.61 ±0.02	0.34 ±0.02	1.11 ±0.11	2.63 ±0.16
5.25 THz	0.90 ±0.03	0.63 ±0.07	1.47 ±0.04	0.56 ±0.02	1.14 ±0.22	4.70 ±0.24

The loss of the lens at each frequency was simulated using COMSOL (see the text), where the error bars originate from the assumption of either loss or no loss in the silicon.

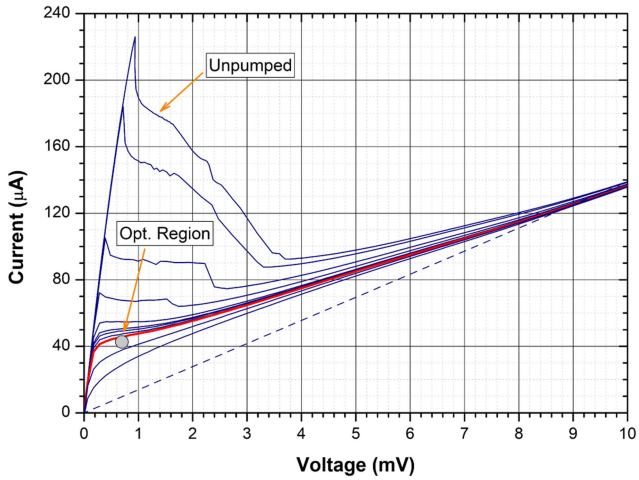

Fig. 2. Unpumped and pumped I–V curves of the NbN HEB at 1.6 THz. The thick red curve represents the optimally pumped I–V. The optimal operating region, within approximately 5% of the lowest $T_{\rm rec}^{\rm DSB}$, is marked with a circle, covering two bias points at 0.6 and 0.8 mV. The dashed load line is used to estimate the LO power at the HEB itself [33].

IV. Results and Discussion

We focus on a single NbN HEB mixer ("OASIS BM2 7B") although two other HEBs from different batches (wafers) have reproduced similar results, showing very comparable sensitivities. A set of measured current–voltage (I–V) curves, both without and with varying LO pumping levels at 1.6 THz, is

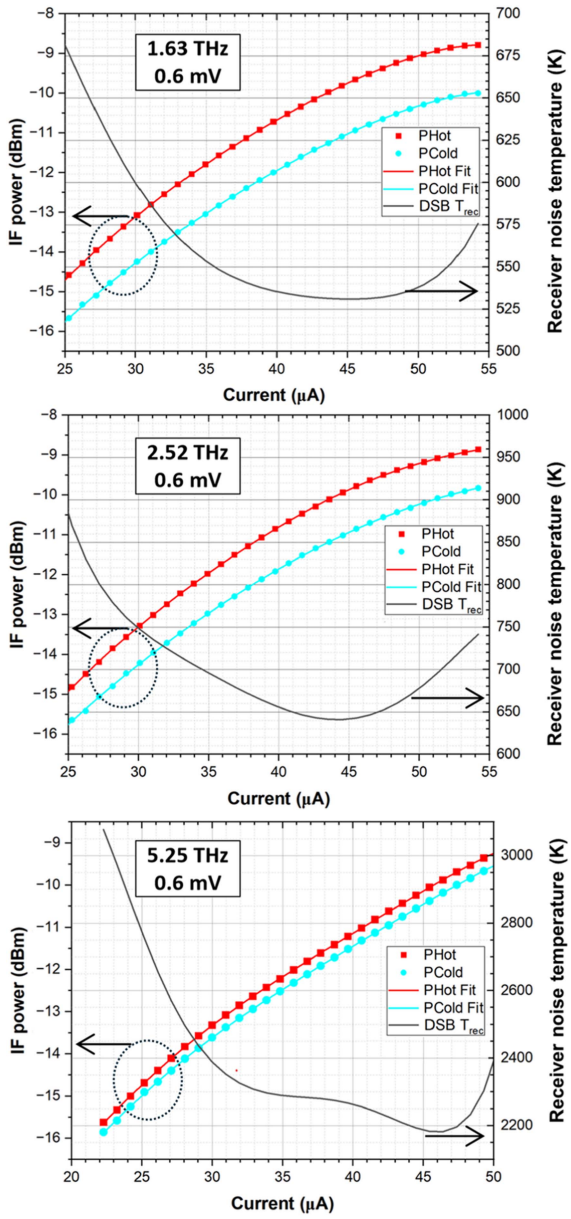

Fig. 3. Measured receiver output power (IF power) in response to hot/cold loads together with the fitted curves (left axis), and DSB receiver noise temperature (right axis) as a function of current at three LO frequencies: 1.6, 2.5, and 5.3 THz, with a bias voltage of 0.6 mV.

presented in Fig. 2, where the optimal operating region resulting in the best $T_{\text{rec}}^{\text{DSB}}$ is indicated.

$T_{\text{rec}}^{\text{DSB}}$ of the mixer is obtained using the *Y*-factor, which is the ratio between the two measured receiver output powers responding to the hot (P_{hot}) and the cold loads (P_{cold}). By combining the *Y*-factor and the Callen–Welton temperatures of the blackbody loads, $T_{\text{rec}}^{\text{DSB}}$ can be obtained [26].

P_{hot} and P_{cold} are recorded as a function of HEB current at an optimal dc bias voltage (0.6 mV), where the current variation reflects the scan of LO power by the voice coil attenuator. We call this measurement method as "the same-current method." In this way, the measurement of $T_{\text{rec}}^{\text{DSB}}$ is not influenced by the fluctuations and drift of the FIR laser power, which is known to occur in

TABLE II
MEASURED DOUBLE SIDEBAND (DSB) RECEIVER NOISE TEMPERATURES ($T_{\text{REC}}^{\text{DSB}}$), DSB RECEIVER CONVERSION LOSSES ($L_{\text{REC}}^{\text{DSB}}$), AND ABSORBED LO POWERS

LO Frequency	$T_{\text{rec}}^{\text{DSB}}$	$L_{\text{rec}}^{\text{DSB}}$	LO power
1.63 THz	530 ± 11 K	6.6 ± 0.08 dB	245 nW
2.52 THz	640 ± 18 K	7.7 ± 0.1 dB	235 nW
5.25 THz	2190 ± 150 K	11.7 ± 0.3 dB	233 nW

FIR gas lasers. This technique can also mitigate the direct detection effect, as referred to the Appendix. Due to stability issues, our FIR gas laser does not allow for reproducible measurements of $T_{\text{rec}}^{\text{DSB}}$ as a function of bias voltage by the fixed-LO-power method, but it does permit the recording of pumped *I–V* curves, as these can be measured within a much shorter time frame.

The measured P_{hot} and P_{cold}, along with the calculated $T_{\text{rec}}^{\text{DSB}}$, are shown for all three frequencies in Fig. 3. The minimum $T_{\text{rec}}^{\text{DSB}}$, observed at a current of around 45 μA, is 530 ± 11 K, 640 ± 18 K, and 2190 ± 150 K at 1.6, 2.5, and 5.3 THz, respectively, with error bars included to account for the uncertainty in the measured receiver output power.

We repeated measurements by varying the voltage up to 1.2 mV in 0.2-mV steps, which yielded practically the same minimum $T_{\text{rec}}^{\text{DSB}}$ values (530, 650, and 2190 K at 1.6, 2.5, and 5.3 THz, respectively) at 0.8 mV, but at a slightly higher current (not shown). These two sets of $T_{\text{rec}}^{\text{DSB}}$ values indicate that the data are consistent and reliable.

We determined the receiver conversion loss ($L_{\text{rec}}^{\text{DSB}}$), or total conversion loss of the mixer, at the same operating points using a standard U-factor technique [27]. The $L_{\text{rec}}^{\text{DSB}}$ values are 6.6 ± 0.08 dB, 7.7 ± 0.1 dB, and 11.7 ± 0.3 dB at 1.6, 2.5, and 5.3 THz, respectively.

We also estimated the absorbed LO power at the HEB from the optimally pumped *I–V* curve using the isothermal technique [28]. P_{LO} is 237 ± 8 nW for all three frequencies and is at least 0.75 μW (1.63 THz), 0.83 μW (2.5 THz), and 1.4 μW (5.3 THz) in front of the cryostat window, calculated considering the relevant optical losses in Table I, the spiral antenna (3 dB), and the antenna–HEB impedance mismatch (to be described later). These LO power values represent a good compromise between the availability of the LO sources and the stability of the receiver. A too high LO power requirement can challenge the LO source, while a too low LO power can make the HEB sensitive to fluctuations in the THz signal and LO power [22]. It is also important to note that we will operate the HEB at a current of $\leq$45 μA for the given voltage (e.g., 0.6 mV). The reason for this will be discussed later. Table II summarizes all the measured receiver performance parameters: $T_{\text{rec}}^{\text{DSB}}$, $L_{\text{rec}}^{\text{DSB}}$, and LO power at the three frequencies.

To fairly assess the mixer performance independent of the measurement setup, we obtain $T_{\text{mixer}}^{\text{DSB}}$ and $L_{\text{mixer}}^{\text{DSB}}$ from the measured receiver parameters, $T_{\text{rec}}^{\text{DSB}}$ and $L_{\text{rec}}^{\text{DSB}}$, in Table II, using the information provided in Table I, as described in [29]. Specifically, for 1.6 THz, we subtract the first four optical loss terms listed in Table I from $L_{\text{rec}}^{\text{DSB}}$, excluding the loss term of the coated

TABLE III
DERIVED DSB MIXER NOISE TEMPERATURE T^{DSB}_{MIXER} AND DSB MIXER CONVERSION LOSS (L^{DSB}_{MIXER}); BOTH INCLUDE THE CONTRIBUTION FROM THE SI LENS, IDEALLY AR COATED FOR EACH SPECIFIC FREQUENCY, AND ANTENNA–HEB IMPEDANCE MISMATCHING LOSS

LO frequency	T^{DSB}_{mixer}	L^{DSB}_{mixer}	T^{DSB}_{mixer} (Quantum noise units)
1.63 THz	240 ± 6 K	4.4 ± 0.09 dB	3.1 × hν/k_B
2.52 THz	290 ± 13K	5.5 ± 0.2 dB	2.4 × hν/k_B
5.25 THz	620 ± 54 K	7.4 ± 0.4 dB	2.5 × hν/k_B

T^{DSB}_{mixer} is in units of hν/k_B (QN). Note that all values are obtained at an IF of 1.7 GHz and an operating temperature of 4.6 K.

Si lens, to determine L^{DSB}_{mixer}. We then apply [29, eq. (1)], using T^{DSB}_{rec}, the noise due to the optics (T_{OP}) of 101 K, the sum of the first four optical loss terms in Table I, and T_{IF} of 6.5 K, to derive T^{DSB}_{mixer}. *It is important to note that both* T^{DSB}_{mixer} and L^{DSB}_{mixer} *include contributions from the optical loss of the AR-coated Si lens (0.35 dB) and the antenna–HEB impedance mismatching loss* (to be discussed).

For the 2.5- and 5.3-THz cases, we derive both T^{DSB}_{mixer} and L^{DSB}_{mixer} from the measured T^{DSB}_{rec} and L^{DSB}_{rec} in Table II and the optical losses in Table I, *assuming that the lens is optimally AR-coated for both frequencies,* resulting in a loss of approximately 0.35 dB. We subtract the modified total optical loss given in Table I, where L_{lens} (the lens optical loss) is 0.35 dB less than stated, from L^{DSB}_{rec} to determine L^{DSB}_{mixer}. We then apply [29, eq. (1)], using T^{DSB}_{rec}, T_{OP} values of 116 K for 2.5 THz and 401 K for 5.3 THz, the modified total optical loss, and T_{IF} of 6.5 K, to derive T^{DSB}_{mixer}. As in the 1.6-THz case, both T^{DSB}_{mixer} and L^{DSB}_{mixer} include contributions from the optical loss of the AR-coated Si lens and the antenna–HEB impedance mismatching loss.

Table III summarizes the mixer performance parameters, namely, T^{DSB}_{mixer} and L^{DSB}_{mixer}, which are likely the lowest values ever reported for HEBs. To provide insight into how close T^{DSB}_{mixer} is to the fundamental noise limit, we also express it in units of the quantum noise (QN, hν/k_B) [9] in this table, where h is Planck's constant, ν is the frequency, and k_B is Boltzmann's constant. We consider Table III to be the key outcome of this article. The errors for T^{DSB}_{mixer} and L^{DSB}_{mixer} are determined using standard error propagation formulas, with the errors based on the total optical losses in Table I and T^{DSB}_{rec} and L^{DSB}_{rec} values in Table II.

Additional useful information is the mixer output noise (T_{out}), which is given by $T^{DSB}_{mixer}/L^{DSB}_{mixer}$. Using the data in Table III, we find T_{out} to be 87, 82, and 113 K at 1.6, 2.5, and 5.3 THz, respectively. These values arise not only from classical noise sources but also include contributions from quantum noise [30], as T^{DSB}_{mixer} contains both components.

It is interesting to note that the same-current method measures a slightly lower (∼10%) T^{DSB}_{rec} compared to the conventional fixed-LO-power method, even for a waveguide HEB [without a cold narrow bandpass filter (CNBPF)], because the latter still suffers from the direct detection effect [31]. Although the same-current method was used in [31], [32], and [33] and in many of the SRON/TU Delft publications, ideally, a CNBPF [26], [34], [35] could be applied to mitigate the direct detection effect. Unfortunately, we do not have ideal CNBPFs available for all three frequencies. However, we do have a 1.6-THz CNBPF from QMC, which has a main transmission peak at 1.59 THz and another broad but much lower peak around 3 THz. At 1.63 THz and 77 K, this filter shows a measured transmission of 75 ± 2%.

We repeated the noise temperature measurements using the same-current method by adding the CNBPF at 4 K. As mentioned earlier, we are unable to use the fixed-LO-power method to measure voltage-dependent T^{DSB}_{rec} curves. In the measurements, we found T^{DSB}_{rec} to be 530 K without the CNBPF and 640 K with the CNBPF. The higher T^{DSB}_{Rec} in the second measurement is believed to be due to the additional optical loss introduced by the CNBPF. We then performed an analysis being same as for the data in Table III and derived T^{DSB}_{mixer} to be 240 K without the CNBPF, and 220 K with the CNBPF. In the second case, we assume that the direct detection effect is minimized, although not eliminated, so the same-current method should provide the same value as the fixed-LO-power method. The observed difference is likely due to an expected increase in the transmission of the CNBPF at 4 K. Assuming a transmission of 83%, the two measurements would show no difference in T^{DSB}_{mixer}. Therefore, we conclude that the same-current method does not overestimate T^{DSB}_{rec} or T^{DSB}_{mixer}. We also noticed that adding a CNBPF not only results in a higher measured T^{DSB}_{Rec} but also introduces additional uncertainty in deriving T^{DSB}_{mixer}.

To better assess the improvements we have made in the HEB, we will compare our T^{DSB}_{mixer} and L^{DSB}_{mixer} values with those reported by others or by our team, if available. When such data are not available, we will compare only T^{DSB}_{rec}. Specifically, we compare T^{DSB}_{mixer} and L^{DSB}_{mixer} with the results obtained from the HEBs used in GUSTO's arrays [14]. These arrays feature spiral antenna-coupled NbN HEBs with dimensions of 0.2 μm × 2 μm and contact structures made of an Nb/Au bilayer. More than 16 HEBs were tested at 1.6 THz, and a similar number was tested at 5.3 THz (from which we extrapolated the 4.7-THz data for GUSTO).

It is important to note that at 1.6 THz, the GUSTO test setup was the same as the one used in this work; therefore, all optical losses are similar. However, all data were measured at an IF of 2 GHz, so we extrapolated the data to 1.7 GHz for comparison. For GUSTO's HEBs, we found the average T^{DSB}_{mixer} and L^{DSB}_{mixer} to be 390 K and 6.7 dB, respectively. In this case, T_{out} is 83 K and will be used in a later discussion. Compared with the T^{DSB}_{mixer} in Table III (240 K), our new result shows a 39% improvement.

No data at 2.5 THz from the HEBs for GUSTO were available for comparison. However, numerous T^{DSB}_{rec} values at this frequency have been published in the literature. For example, a T^{DSB}_{rec} of 600–900 K, measured within 1.3–2 GHz at IF, was reported for an HEB with in situ fabricated Au/NbN contacts [17]. These data, however, show large variation and could also be interpreted as $T^{DSB}_{rec} = 750 \pm 150$ K.

Other examples include a T^{DSB}_{rec} of 780 K reported in [36], which used Ar^+-cleaned Au/NbN contacts [18], 900 K in [37], 1400 K in [38], and 630 K in [22], all measured in a similar setup but in vacuum [26] at SRON, implying less optical loss than our setup in air (e.g., no losses from air and window). In addition, 1100 K was reported in an air setup in [39], 950 K in [40], and 1800 K in [41], the latter being measured earlier in an Nb diffusion-cooled HEB.

Therefore, we can generally conclude that our new $T_{\text{rec}}^{\text{DSB}}$ at 2.5 THz is at least 30% lower than what has been reported so far in the literature [36], [37], [38], [39], [40], [41]. Here, we compare $T_{\text{rec}}^{\text{DSB}}$ rather than $T_{\text{mixer}}^{\text{DSB}}$ because the latter is often not available in the literature or cannot be derived due to missing information.

At 5.3 THz, the HEBs for GUSTO have shown an average $T_{\text{mixer}}^{\text{DSB}}$ of 760 K and $L_{\text{mixer}}^{\text{DSB}}$ of 9.3 dB at an IF of 1.7 GHz [14]. The new $T_{\text{mixer}}^{\text{DSB}}$ of 620 K shows an 18% improvement, which is marginal. We also compare our new $T_{\text{rec}}^{\text{DSB}}$ value (2190 K) at 5.3 THz with those reported in the literature, specifically in [19] and [42], using the vacuum setup at SRON, after correcting for differences in optical loss. In comparison with these cases, the improvement is almost negligible.

The smaller improvement in $T_{\text{mixer}}^{\text{DSB}}$ at 5.3 THz may be partly due to the quantum noise, which plays a more significant role as the frequency increases [30].

There are additional measured performance data of HEBs in the literature. However, due to differences in LO frequency, we do not provide a detailed comparison here but quote some recent results of measured $T_{\text{rec}}^{\text{DSB}}$: 700 K at 1.9 THz (at 1.7 GHz IF) [43], and 950 K at 4.75 THz (at an IF between 1.25 and 1.75 GHz) [31].

Here, we aim to address possible questions that might arise from the measured data. First, why does $L_{\text{mixer}}^{\text{DSB}}$ in Table III increase by 3 dB from 1.6 THz to 5.3 THz? We believe that this is due to an increase in the antenna–HEB impedance mismatching loss. This is caused by the modification of the antenna to accommodate a 4-μm-wide NbN bridge, resulting in a less tightly wound structure than the antenna used in [19] and [20], which has an inner diameter of 6.6 μm and performs well at higher frequencies. In contrast, the antenna used here has an inner diameter of 12 μm, which is less favorable for 5.3 THz [44].

To discuss this quantitatively, we simulated the impedance mismatching loss for our case using COMSOL, in the same manner as in [19]. We found the impedance mismatching loss to be 0.13, 0.36, and 1.6 dB for 1.6, 2.5, and 5.3 THz, respectively. The loss at 5.3 THz is significantly higher than that of the antenna used in [19] and [20] (0.63 dB), which can explain a large portion of the increase in $L_{\text{mixer}}^{\text{DSB}}$ in Table III.

To further quantify this, we calculated the intrinsic DSB mixer conversion loss ($L_{\text{mixer}}^{\text{DSB, intrin}}$) using the data for $L_{\text{mixer}}^{\text{DSB}}$ from Table III, by subtracting the antenna–HEB impedance mismatching losses and the 0.35-dB loss for coated Si lenses at all three frequencies. We found that $L_{\text{mixer}}^{\text{DSB, intrin}}$ is 3.9, 4.8, and 5.4 dB for 1.6, 2.5, and 5.3 THz, respectively. These values are considerably lower than those reported in [30] and are lower than other values reported for THz HEBs, as far as we know. However, the remaining increase in $L_{\text{mixer}}^{\text{DSB, intrin}}$, which was also observed in [30], is unexpected.

We expect $L_{\text{mixer}}^{\text{DSB, intrin}}$ to be frequency independent within the range of our experiment, where THz photon energies are significantly higher than the gap frequency of the NbN bridge. This expectation is supported by the close-to-optimally pumped *I–V* curves at the three frequencies, which overlap extremely well, as shown in Fig. 4. This result suggests that the effect of THz current heating in the bridge is same across all three frequencies.

Furthermore, we speculate that, despite the wide NbN HEB (4 μm), the flow of THz current along the bridge is likely uniform, similar to what was observed for a narrower NbN HEB (2 μm) [45]. This is particularly interesting because the skin depth for the NbN at 5.3 THz is 0.43 μm, which is only about 10% of the bridge width.

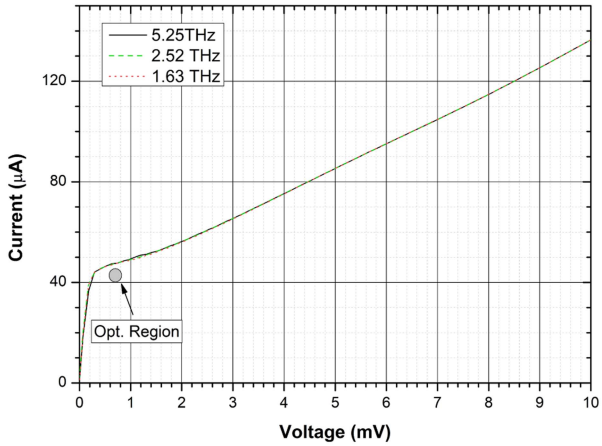

Fig. 4. Close-to-optimally pumped *I–V* curves of the NbN HEB at three frequencies 1.6, 2.5, and 5.3 THz appear to be fully overlapped.

As a byproduct of this discussion, we can state that it is still valid to apply the normal state resistance as the RF impedance of the 4-μm HEB at a high frequency of 5.3 THz.

The enhanced sensitivity of the NbN HEB mixer, indicated by a reduced $T_{\text{mixer}}^{\text{DSB}}$, is primarily due to the reduction of $L_{\text{mixer}}^{\text{DSB}}$ compared to GUSTO's HEBs, which use Nb/Au bilayer contact structures. This is evident since T_{out} from both types of HEBs is similar (87 K versus 83 K) when focusing on the 1.6-THz data. $L_{\text{mixer}}^{\text{DSB}}$ in Table III at 1.6 THz is roughly 2 dB lower than that found for GUSTO's HEBs. We attribute the reduction of $L_{\text{mixer}}^{\text{DSB}}$ to the following aspects of our contacts: a) the transparent contacts in our HEBs, together with a wider bridge width of 4 μm, eliminate any contact resistance; b) the use of thick Au contacts; both a) and b) can reduce RF loss and thus $L_{\text{mixer}}^{\text{DSB}}$; and c) the transparent and thick Au contacts can alter the temperature profile of the hot electrons across the bridge, affecting the *I–V* characteristics. According to the hot spot model of mixing for an HEB [46], [47], [48], the mixer conversion loss and noise are influenced by these temperature changes, potentially reducing $L_{\text{mixer}}^{\text{DSB}}$. Our improved $T_{\text{mixer}}^{\text{DSB}}$ confirms experimentally that the contacts play a crucial role, though this is not yet fully understood theoretically. Therefore, other unknown effects cannot be ruled out.

The reduced $L_{\text{mixer}}^{\text{DSB}}$ can further decrease the noise contribution of an LNA (refer to [29, eq. (1)]) and thus lower the receiver (or system) noise temperature of a practical instrument.

Our contacts behave differently from the earlier Au-to-NbN contacts [15], [40], which do not change T_c of the contact region or the NbN bridge. This suggests poor interfaces because of the absence of Ar^+ cleaning.

The enhanced sensitivity of the NbN HEB mixer through contact engineering, as reported here, can also inspire the development of novel MgB_2 HEB mixers [29], [49], [50], which can offer a high operating temperature of $\geq$ 20 K and a large IF bandwidth of $\geq$ 10 GHz. However, little research has been conducted on optimizing the contacts [21].

The optimal operating region of the HEB is indicated in Fig. 2. More specifically, at 0.6 mV, we choose to operate the HEB at a current of 45 μA or below, as suggested by Fig. 3. Operating at a current above 45 μA should be avoided because it shifts away from the resistive state, where the HEB is known to be unstable [51] and prone to relaxation oscillations that switch between the superconducting and resistive states [52]. Such oscillations have also been recently reported in [53]. The same study found weaker intrinsic oscillations when an NbN HEB is in the resistive state without LO power and is operated near its T_c. Although it is unclear whether these intrinsic oscillations affect the performance of the HEB, it might be valuable to conduct dedicated measurements to identify the region of low $T_{\mathrm{rec}}^{\mathrm{DSB}}$ free of any unwanted oscillations.

V. Conclusion

By introducing cleaned thick Au contacts to an NbN HEB mixer, we have demonstrated extremely low mixer noise temperatures $T_{\mathrm{mixer}}^{\mathrm{DSB}}$ of 240 and 290 K at 1.6 and 2.5 THz, respectively, which are approximately three times the quantum noise ($h\nu/k_B$). All the $T_{\mathrm{mixer}}^{\mathrm{DSB}}$ values account for contributions from both the optical loss of the AR-coated Si lens and the antenna–HEB impedance mismatching loss. The improvement in $T_{\mathrm{mixer}}^{\mathrm{DSB}}$ exceeds 30% in comparison with reported NbN HEB mixers [14], potentially reducing the integration time of a heterodyne instrument by roughly a factor of 2. In other words, this enhancement can double the observation speed, which is highly advantageous for cryogenic space missions with the limited lifetime.

$T_{\mathrm{mixer}}^{\mathrm{DSB}}$ of the same HEB at 5.3 THz has been measured and shown 620 K, showing a more limited improvement. This is partly attributed to the nonoptimized antenna geometry, supported by high antenna–HEB impedance mismatching, and partly due to the quantum noise at this high frequency. Interestingly, despite the 4-μm-wide NbN bridge, the pumped *I–V* curves are identical at the three frequencies, suggesting that the RF current flows uniformly along the bridge.

This mixer is developed for future FIR space observatories, particularly for the SALTUS mission concept, for which a proposal has been submitted to NASA in response to the Probe mission call.

Appendix

The technique of using the same-current method to determine the *Y*-factor can mitigate the direct detection effect [26], [32], [33] and thus reduce its impact on $T_{\mathrm{rec}}^{\mathrm{DSB}}$. Essentially, the same current is achieved by slightly adjusting the LO power (P_{LO}) to compensate for the difference between the broadband hot and cold load power. Consequently, the bias points in both cases are made identical, although P_{LO} is no longer the same. Conceptually, this is not fully accurate because of the difference in mixer gain [47], [54].

However, in the practical case of an NbN HEB, as discussed in this work, where the change in P_{LO} is small (only 2–4% of the required P_{LO}, this method effectively mitigates the direct detection effect without overestimating $T_{\mathrm{rec}}^{\mathrm{DSB}}$. This conclusion is based on our earlier experiments in [26] and [35], where we compared the same-current method with the conventional fixed-LO-power method, in which a CNBPF centered at the LO frequency was introduced.

Acknowledgment

The authors would like to thank Yuner Gan for modeling the loss of the AR-coated Si lens. The authors would also like to acknowledge Marc Zuiddam and the staff at Kavli Nanolab Delft for their technical support. The authors are grateful for the invaluable support from Paul Urbach at TU Delft, as well as Pieter Dieleman, Jan-Willem den Herder, and Jan Geralt bij de Vaate at SRON.

References

[1] S. Cherednichenko, V. Drakinskiy, T. Berg, P. Khosropanah, and E. Kollberg, "Hot-electron bolometer terahertz mixers for the Herschel Space Observatory," *Rev. Sci. Instrum.*, vol. 79, no. 3, Mar. 2008, Art. no. 034501.
[2] C. Risacher et al., "The upGREAT dual frequency heterodyne arrays for SOFIA," *J. Astron. Instrum.*, vol. 7, no. 4, Dec. 2018, Art. no. 1840014.
[3] Y. M. Seo et al., "Probing ISM structure in Trumpler 14 and Carina I using the stratospheric terahertz observatory 2," *Astrophys. J.*, vol. 878, no. 2, Jun. 2019, Art. no. 120.
[4] C. Walker et al., "Gal/Xgal U/LDB Spectroscopic/Stratospheric THz Observatory: GUSTO," *Proc. SPIE*, vol. 12190, 2022, Art. no. 121900E.
[5] J. V. Siles et al., "ASTHROS: The astrophysics stratospheric telescope for high spectral resolution observations at submillimeter-wavelengths," *Proc. SPIE*, vol. 11445, 2020, Art. no. 114453G.
[6] D. Rigopoulou et al., "The far-infrared spectroscopic surveyor (FIRSS). Experimental astronomy," *Exp. Astron.*, vol. 51, no. 3, pp. 699–728, May 2021.
[7] C. K. Walker et al., "Orbiting Astronomical Satellite for Investigating Stellar Systems (OASIS): Following the water trail from the interstellar medium to oceans," *Proc. SPIE*, vol. 11820, 2021, Art. no. 118200O.
[8] G. Chin et al., "Single aperture large telescope for universe studies (SALTUS): Science overview," 2024, *arXiv:2405.12829*.
[9] C. K. Walker, *Terahertz Astronomy*. New York, NY, USA: Taylor & Francis, 2016.
[10] H.-W. Hubers, "Terahertz Heterodyne receivers," *IEEE J. Sel. Top. Quantum Electron.*, vol. 14, no. 2, pp. 378–391, Apr. 2008.
[11] A. Shurakov, Y. Lobanov, and G. Goltsman, "Superconducting hot-electron bolometer: From the discovery of hot-electron phenomena to practical applications," *Supercond. Sci. Technol.*, vol. 29, no. 2, Dec. 2015, Art. no. 023001.
[12] T. M. Klapwijk and A. V. Semenov, "Engineering physics of superconducting hot-electron bolometer mixers," *IEEE Trans. THz Sci. Technol.*, vol. 7, no. 6, pp. 627–648, Oct. 2017.
[13] X. Liu, "Demonstration of 2×2 heterodyne receiver array at 1.4THz using HEB mixers and Fourier phase grating LO," M.S. thesis, Dept. Microelectronics, Delft Univ. Technol., Delft, The Netherlands, 2015.
[14] J. R. G. Silva et al., "4×2 Hot electron bolometer mixer arrays for detection at 1.46, 1.9 and 4.7 THz for a balloon-borne terahertz observatory," 2023, *arXiv:2311.05755*.
[15] M. Hajenius et al., "Low noise NbN superconducting hot electron bolometer mixers at 1.9 and 2.5 THz," *Supercond. Sci. Technol.*, vol. 17, pp. S224–S228, Mar. 2004.
[16] T. Aggarwal et al., "Superconducting contacts and NbN HEB mixer performance," in *Proc. 19th Int. Symp. Space THz Technol.*, Groningen, The Netherlands, 2008, pp. 398–402.
[17] I. Tretyakov et al., "Low noise and wide bandwidth of NbN hot-electron bolometer mixers," *Appl. Phys. Lett.*, vol. 98, 2011, Art. no. 033507.
[18] R. Lefèvre et al., "Terahertz NbN hot electron bolometer fabrication process with a reduced number of steps," in *Proc. 23rd Int. Symp. Space THz Technol.*, Tokyo, Apr. 2012, pp. 122–125.
[19] W. Zhang et al., "Noise temperature and beam pattern of a NbN hot electron bolometer mixer at 5.25 THz," *J. Appl. Phys.*, vol. 108, no. 9, Nov. 2010, Art. no. 093102.
[20] J. R. G. Silva et al., "Beam waist properties of spiral antenna coupled HEB mixers at supra-THz frequencies," *IEEE Trans. THz Sci. Technol.*, vol. 13, no. 2, pp. 167–177, Mar. 2023.

[21] Y. Gan et al., "Heterodyne performance and characteristics of terahertz MgB_2 hot electron bolometers," *J. Appl. Phys.*, vol. 133, no. 7, Feb. 2023, Art. no. 074503.
[22] D. J. Hayton et al., "Stabilized hot electron bolometer heterodyne receiver at 2.5 THz," *Appl. Phys. Lett.*, vol. 100, no. 8, Feb. 2012, Art. no. 081102 (see footnote 19 there).
[23] A. J. Gatesman, J. Waldman, M. Ji, C. Musante, and S. Yagvesson, "An anti-reflection coating for silicon optics at terahertz frequencies," *IEEE Microw. Guided Wave Lett.*, vol. 10, no. 7, pp. 264–266, Jul. 2000.
[24] H. W. Hüber et al., "Parylene anti-reflection coating of a quasi-optical hot-electron bolometric mixer at terahertz frequencies," *Infrared Phys. Technol.*, vol. 42, no. 1, pp. 41–47, 2001.
[25] D. Grischkowsky, S. Keiding, M. van Exter, and C. Fattinger, "Far-infrared time-domain spectroscopy with terahertz beams of dielectrics and semiconductors," *J. Opt. Soc. Amer. B*, vol. 7, no. 10, 1990, Art. no. 2006.
[26] P. Khosropanah, J. R. Gao, W. M. Laauwen, and M. Hajenius, "Low noise NbN hot electron bolometer mixer at 4.3 THz," *Appl. Phys. Lett.*, vol. 91, no. 22, Nov. 2007, Art. no. 221111.
[27] S. Cherednichenko et al., "1.6 THz heterodyne receiver for the far infrared space telescope," *Phys. C, Supercond. Appl.*, vol. 427, pp. 427–431, Mar. 2002.
[28] H. Ekström, B. S. Karasik, E. Koll erg, and K. S. Yngvesson, "Conversion gain and noise of niobium superconducting hot-electron-mixers," *IEEE Trans Microw. Theory Techn.*, vol. 43, no. 4, pp. 938–947, Apr. 1995.
[29] Y. Gan et al., "Low noise MgB2 hot electron bolometer mixer operated at 5.3 THz and 20 K," *Appl. Phys. Lett.*, vol. 119, no. 20, Nov. 2021, Art. no. 202601.
[30] W. Zhang et al., "Quantum noise in a terahertz hot-electron bolometer mixer," *Appl. Phys. Lett.*, vol. 96, no. 11, Mar. 2010, Art. no. 111113.
[31] D. Büchel et al., "4.7-THz superconducting hot-electron bolometer waveguide mixer," *IEEE Trans. THz Sci. Technol.*, vol. 5, no. 2, pp. 207–214, Mar. 2015.
[32] S. Svechnikov et al., "Quasioptical phonon-cooled NbN hot-electron bolometer mixer at 0.5–1.1 THz," in *Proc. 9th Int. Symp. Space THz Technol.*, Pasadena, CA, USA, 1998, pp. 45–53.
[33] S. Cherednichenko, V. Drakinsky, T. Berg, E. L.Kollberg, and I. Angekov, "The direct detection effect in the hot-electron bolometer mixer sensitivity calibration," *IEEE Trans Microw. Theory Techn.*, vol. 55, no. 3, pp. 504–510, Mar. 2007.
[34] J. J. A. Baselmans et al., "Direct detection effect in small volume hot electron bolometer mixers," *Appl. Phys. Lett.*, vol. 86, no. 16, 2005, Art. no. 163503.
[35] M. Hajenius et al., "Full characterization and analysis of a terahertz heterodyne receiver based on a NbN hot electron bolometer," *J. Appl. Phys.*, vol. 100, Oct. 2006, Art. no. 074507.
[36] Y. Delorme et al., "A quasi-optical NbN HEB mixer with 800 K DSB noise temperature at 2.5 THz," in *Proc. 22nd Int. Symp. Space THz Technol.*, Tucson, AZ, USA, 2011, pp. 123–126.
[37] W. Zhang et al., "Twin-slot antenna coupled NbN hot electron bolometer mixer at 2.5 THz," *IEEE Trans. THz Sci. Technol.*, vol. 1, no. 2, pp. 378–382, Nov. 2011.
[38] P. Pütz et al., "Terahertz hot electron bolometer waveguide mixers for GREAT," *Astron. Astrophys.*, vol. 542, Jun. 2012, Art. no. L2.
[39] M. Kroug et al., "NbN hot electron bolometric mixers for terahertz receivers," *IEEE Trans. Appl. Supercond.*, vol. 11, no. 1, pp. 962–965, Mar. 2001.
[40] J. J. A. Baselmansa et al., "Doubling of sensitivity and bandwidth in phonon cooled hot electron bolometer mixers," *Appl. Phys. Lett.*, vol. 84, no. 11, pp. 1958–1961, Mar. 2004.
[41] R. A. Wyss, B. S. Karasik, W. R. McGrath, B. Bumble, and H. LeDuc, "Noise and bandwidth measurements of diffusion-cooled Nb hot-electron bolometer mixers at frequencies above the superconductive energy gap," in *Proc. 10th Int. Symp. Space THz Technol.*, Charlottesville, VA, USA, 1999, pp. 215–228.
[42] J. L. Kloosterman et al., "Hot electron bolometer heterodyne receiver with a 4.7-THz quantum cascade laser as a local oscillator," *Appl. Phys. Lett.*, vol. 102, no. 1, Jan. 2013, Art. no. 011123.
[43] C. Risacher et al., "First supra-THz heterodyne array receivers for astronomy with the SOFIA observatory," *IEEE Trans. THz Sci. Technol.*, vol. 6, no. 2, pp. 199–211, Mar. 2016.
[44] A. D. Semenov et al., "Terahertz performance of integrated lens antennas with a hot-electron bolometer," *IEEE Trans. Microw. Theory Techn.*, vol. 55, no. 2, pp. 239–247, Feb. 2007.
[45] E. L. Kollberg et al., "Impedance of hot-electron bolometer mixers at terahertz frequencies," *IEEE Trans. THz Sci. Technol.*, vol. 1, no. 2, pp. 383–389, Nov. 2011.
[46] D. Wilms Floet, E. Miedema, T. M. Klapwijk, and J. R. Gao, "Hotspot mixing: A framework for heterodyne mixing in superconducting hot-electron bolometers," *Appl. Phys. Lett.*, vol. 74, pp. 433–435, Jan. 1999.
[47] H. F. Merkel, P. Khosropanah, D. W. Floet, P. A. Yagoubov, and E. L. Kollberg, "Conversion gain and fluctuation noise of phonon-cooled hot-electron bolometers in the hot-spot regime," *IEEE Trans. Microw. Theory Techn.*, vol. 48, no. 4, pp. 690–699, Apr. 2000.
[48] W. Miao et al., "Investigation of the performance of NbN superconducting HEB mixers of different critical temperatures," *IEEE Trans. Appl. Supercond.*, vol. 27, no. 4, Jun. 2017, Art. no. 2200304.
[49] E. Novoselov and S. Cherednichenko, "Low noise terahertz MgB_2 hot-electron bolometer mixers with an 11 GHz bandwidth," *Appl. Phys. Lett.*, vol. 110, no. 3, Jan. 2017, Art. no. 032601.
[50] D. Cunnane et al., "Optimization of parameters of MgB_2 hot-electron bolometers," *IEEE Trans. Appl. Supercond.*, vol. 27, no. 4, Jun. 2017, Art. no. 2300405.
[51] A. D. Semenov et al., "Design and performance of the lattice-cooled hot-electron terahertz mixer," *J. Appl. Phys.*, vol. 88, no. 11, 2000, Art. no. 6758.
[52] Y. Zhuang and K. S. Yngvesson, "Detection and interpretation of bistability effects in NbN HEB devices," in *Proc. 13th Int. Symp. Space THz Technol.*, 2002, pp. 463–472.
[53] R. F. Su et al., "Microwave probing of relaxation oscillations related to terahertz power detection in superconducting hot electron bolometers," *Supercond. Sci. Technol.*, vol. 32, 2019, Art. no. 105002.
[54] B. S. Karasik and A. I. Elantev, "Noise temperature limit of a superconducting hot-electron bolometer mixer," *Appl. Phys. Lett.*, vol. 68, no. 6, pp. 853–855, 1996.

Behnam Mirzaei received the Ph.D. degree in applied physics from the Delft University of Technology, Delft, The Netherlands, in 2018.

He was a Postdoctoral Researcher with the Delft University of Technology. He was with SRON Netherlands Institute for Space Research, Leiden, The Netherlands, for two years. During and after his Ph.D. research, he contributed to the development of terahertz (THz) heterodyne receivers. He worked on THz quantum cascade lasers, which are used as local oscillators. He developed a phase grating as THz beam multiplexer for GUSTO. He worked on MgB_2 Hot Electron Bolometer Mixers for future space missions, where he could considerably improve the sensitivity. His research outcomes have been published in several scientific articles.

Jose R. G. Silva received the Ph.D. degree in astronomy from the University of Groningen, Groningen, The Netherlands, in 2022.

Since 2016, he has been a Researcher with SRON Netherlands Institute for Space Research (SRON), Groningen, The Netherlands, with a focus on developing heterodyne detector arrays based on the superconducting hot electron bolometer at terahertz frequencies, having contributed to the NASA balloon-borne telescope GUSTO. He is an Instrument Scientist with SRON, working on both heterodyne technology and direction detection with a focus on microwave kinetic inductance detectors.

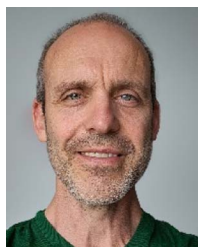

Willem-Jan Vreeling received the Engineering degree in applied physics from Hogeschool Enschede, Enschede, The Netherlands, in 1999.

He started his career as a Physics Research Assistant with SRON Netherlands Institute for Space Research (SRON), Groningen, The Netherlands. At SRON, he worked for general laboratory support and on heterodyne projects. In early 2000s, he worked for a few years in the field of remote sensing with the German Aerospace Center, Oberpfaffenhofen, Germany, where he was an Engineer with the Calibration Laboratory and for the airworthiness certification. In 2009, he returned to SRON and continued his work as a Physics Research Assistant. Since then, he has been supporting several projects, such as SAFARI, ATHENA, PLATO, and SALTUS.

Wouter M. Laauwen received the Engineering degree in applied physics from Hogeschool Eindhoven, Eindhoven, The Netherlands, in 1994.

In mid-2000s, he followed dedicated training in Systems Engineering and Requirements Specification writing and analysis. He started his career as a Lithography Engineer with the Thin Film Physics Group, University of Groningen, Groningen, The Netherlands, where he worked on applying then-novel technologies such as deep-ultraviolet and e-beam for nanometer-scale devices to investigate fundamental properties of superconductive- and spin-polarized transport. Since 1998, he has been with the Instrument Science Group, Netherlands Institute for Space Research, Groningen, The Netherlands. He involved in the development of the HIFI-Herschel band 3 and 4 superconductor–insulator–superconductor mixers, which evolved into the role of HIFI focal plane specialist. After the delivery of the HIFI flight instrument, he worked as a Systems Engineer/Instrument Scientist for a broad range of projects such as SAFARI (Calibration and AIV), Spex Airborne (calibration and pointing reconstruction), STO2 (all detectors), GUSTO (all detectors and 4.7-THz LO system), PLATO (Camera—TVAC facility and Testing) SALTUS (SAFARI-lite instrument), and LISA (QPR development).

Dingding Ren received the Ph.D. degree in nanoelectronics and photonics from the Norwegian University of Science and Technology (NTNU), Trondheim, Norway, in 2017.

He was a Postdoctoral Researcher with both NTNU and the University of Notre Dame, Notre Dame, IN, USA. Later, he was a Full-Time Researcher with NTNU, leading a three-year Research Council project focused on developing low-loss integrated photonics in the long-wave infrared. He is currently a Postdoctoral Scientist with the Delft University of Technology, Delft, The Netherlands, where he is working on the integration of metalens technology with terahertz hot electron bolometer mixers as part of the EU Radioblock project.

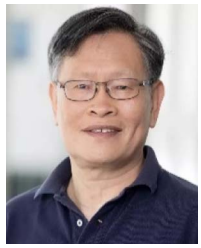

Jian-Rong Gao received the B.Sc. and M.Sc. degrees in physics from Fudan University, Shanghai, China, in 1982 and 1985, respectively, and the Ph.D. degree in applied physics from the Delft University of Technology (TU Delft), Delft, The Netherlands, in 1991.

He was a Postdoctoral Researcher with the University of Groningen, Groningen, The Netherlands. He is currently a Senior Instrument Scientist as well as a Section Manager with The Netherlands Institute for Space Research (SRON), Leiden, The Netherlands. He is also an Associate Professor with the Department of Imaging Physics and the Delft Space Institute, TU Delft. He has supervised eight Ph.D. students and many postdoctoral researchers. He has led several collaborative projects between SRON and TU Delft, notably the NASA STO2 balloon-borne terahertz (THz) observatory (2016) and the GUSTO balloon-borne THz observatory (2023). He has authored or coauthored more than 320 papers in various subjects, including superconducting NbN or MgB_2 hot electron bolometer (HEB) mixers, HEB arrays, THz quantum cascade lasers, THz Fourier phase gratings, THz wavefront sensors, THz beam filters, THz metasurfaces, transition edge sensors (TES) for far infrared and X-ray, frequency-domain multiplexing for TES arrays, space instrumentation, kinetic inductance detectors (KIDs), superconductor–insulator–superconductor mixers, superconductor/2-D electron gas structures, and nano MOSFET structures and physics.